



**Skin Cancer Prediction Model Based on Multi-Layer Perceptron
Network**

Sumangala B*

*Department of Computer Science, Sri Venkateswara, College of Engineering Bangalore
India.bsuma.vijay@gmail.com*

Kavitha B N

*Department of Mathematics, Sri Venkateswara, College of Engineering Bangalore, India
kavithabn103@gmail.com*

Kulkarni Varsha

*Department of Computer Science, Sri Venkateswara, College of Engineering, Bangalore,
India*

vakulkarni73@gmail.com

Vikas H

*Department of Electronics & Communication Engineering, Sri Venkateswara College of
Engineering, Bangalore, India*

vikasvicky.hr@gmail.com

Pavan P Kashyap

*Department of Computer Science & Engineering- Cyber Security, Sri Venkateswara,
College of Engineering, Bangalore, India
pavanpk045@gmail.com*

Article History	Abstract
Received: 1 October 2023 Revised: 15 November 2023 Accepted: 6 December 2023	Melanoma is acknowledged by the World Health Organization as the most severe type of skin cancer, significantly contributing to skin cancer-related deaths worldwide. This type of cancer manifests through noticeable changes in moles, including their size, shape, colour, or texture. In this study, we introduce an innovative and robust method for detecting and classifying melanoma in various image types, including both basic and clinical dermatological images. Our approach employs the HSV (Hue, Saturation, and Value) colour model, along with mathematical morphology and Gaussian filtering techniques. These methods are used to pinpoint the area of interest in an image and compute four key descriptors crucial for melanoma analysis: symmetry, border irregularity, colour variation, and dimension. Despite the prior usage of these descriptors over an extended period, the manner in which they are calculated in this proposal is a key factor contributing to the improvement of the outcomes. Following this, a multilayer perceptron is utilized for the purpose of categorizing malignant and benign melanoma. The study included three datasets consisting of basic and dermatological photographs that are frequently referenced in academic literature. These datasets were applied to both train and assess the effectiveness of the proposed technique. Based on the results obtained from k-fold cross-validation, it is evident that the proposed model surpasses three existing state-of-the-art approaches. In particular, the model demonstrates remarkable precision, with an accuracy rate of 98.5% for basic images and 98.6% for clinical dermatological images. It exhibits a high level of

<p>CC License CC-BY-NC-SA 4.0</p>	<p>sensitivity, measuring 96.68% for simple images and 98.05% for dermatological images. Additionally, its specificity stands at 98.15% when analyzing basic images and 98.01% for dermatological images, indicating its effectiveness in both types of image analysis. The findings have demonstrated that the utilization of this gadget as an assistive tool for melanoma diagnosis would enhance levels of reliability in comparison to traditional methods.</p> <p>Keywords: <i>Melanoma, Basal Cell Carcinoma, Deep Learning, Convolutional Neural Network, Skin Lesion, Segmentation, Classification</i></p>
--	--

1. Introduction

In the 21st century, dermatological diseases are a major medical problem because of the difficulty and subjectivity of human interpretation. When it comes to human health, the skin is by far the most vital organ. The skin's job is to keep the muscles, bones, and internal organs safe from harm. The skin plays a critical role in shielding the body from the damaging effects of ultraviolet (UV) radiation. DNA damage occurs in skin cells due to the sun's UV radiation. These may cause skin disorders and any type of skin cancer. Melanin is present in the skin cells to protect the skin from the sun's harmful rays [1].

For this reason, pale skin is more vulnerable to the sun's harmful ultraviolet rays than dark skin. That is why melanoma patients with pale skin are so prevalent. It has been found that melanoma cancer is the most deadly form of skin disease in humans. There are two primary forms of melanoma: malignant and non-malignant. Malignant, the most lethal and severe form of skin cancer, melanoma, affects only 4% of the population. However, it is responsible for 75% of the deaths caused by the disease among those diagnosed. Doctors can preserve the lives of patients diagnosed with skin cancer at an early stage, but those diagnosed at a later stage are at greater risk of having their skin cancer spread and become more dangerous. In more advanced stages, getting rid of it will be more challenging. Melanoma is caused by the proliferation of melanocytes, which can be found in all body parts. Prompt and accurate diagnosis of skin cancer is made possible by the Biopsy method. In this method, a human tissue sample is extracted and sent to a lab for testing. To do this, one must undergo a lengthy, arduous, and painful undertaking. This will take a long time for testing purposes. Diagnostic testing necessitates more time for both patients and doctors. Because a biopsy raises the likelihood of the disease spreading to other areas, it is more dangerous to perform one [2].

As a primary outcome of the work done, we hope to raise the quality and accuracy of medical diagnosis as a result of our efforts. A primary characteristic of medical imaging is its difficulty in providing data that can be properly processed [3]. In the images, there is a significant quantity of noise and a wide range of attributes. To improve the quality of the final image, the picture attributes are extracted or isolated during the image processing process. This discipline has had a significant impact on a variety of fields, including medicine, telecommunications, process control in manufacturing, and entertainment [4]. Image processing has been shown to be beneficial in the detection of melanoma in the literature [5]. There are two types of melanomas: melanoma and non-melanoma. Melanoma develops in cells called melanocytes, which produce melanin (the pigment that gives skin its colour) [6], [7]. It is used by the American Academy of Dermatology to diagnose melanoma. It was first proposed in 1985 that the ABCD rule should be followed while attempting to identify objects. Where A: Symmetry, B: Edge, C: Color, and D: Size.

Most skin malignancies are not melanomas, rather basal cell carcinoma (BCC) and squamous cell carcinoma (SCC) are far more frequent. These three forms of skin cancer typically manifest in the epidermis's middle and higher layers. The likelihood of this malignancy spreading to other parts of the body is quite low. Melanoma is a very challenging cancer to treat, while non-melanoma tumours are typically easier to deal with. Consequently, the most crucial aspect of treating skin cancer is detecting it early [8], [9].

Recent advances in computer vision-based computation approaches have had a substantial impact on medical imaging analysis as a whole. Deep skin and tissue examination have been made

possible by improvements in resolution in many modern medical image equipment, primarily in the diagnosis and detection of keratinocyte skin cancers. The gold standard for diagnosing actinic keratosis (AK) is still skin biopsy and histological investigations [10], [11].

The use of clinical pictures to detect keratinocyte premalignancy has been the subject of numerous research. Hames et al. [11] presented the identification of erythema using colour space transformations and morphological features, while Ballerini et al. [12] proposed KNN-based clustering to distinguish benign and malignant lesions. Fuzzy logic was used by N. Georgopoulos et al. [13] to construct a specific C-means logic that uses exponent selection to identify the vermilion border between diseased and healthy lips. An automated technique for detecting and diagnosing pigmented skin lesions and melanoma was proposed by Fernandez Alcon et al. [14]. Graph theory was used as a methodology. Additional filtering algorithms for network directional detection in a coloured manner have been presented [16].

In order to prevent the advancement of AK to an advanced malignant state, our study aims to identify and describe such lesions in the early stages. Machine learning approaches are used to identify and classify lesions associated with AK and basal cell carcinoma (BCC) based on their texture features, which are then evaluated based on their ability to classify the lesions.

The first section of this research work briefly covers the prevalence and disease burden of AK, BCC, and Squamous cell carcinoma (SCC) disorders, followed by several computational techniques used in finding and classifying lesions in the following sections. The second section discusses the literature survey carried out to find the existing methods. The third section explains the proposed methodology for identifying and detecting skin cancer using Multi-Layer Perceptron (MLP) computational methods for segmenting, identifying, and characterizing lesions. This is followed by the approach and results, which show the stages of implementation and the validated results obtained. At last, the research work concludes with a discussion of the findings and validation with k crossfold.

2. Related Works

Skin cancer is a significant public health concern, and the development of accurate and efficient diagnostic tools is critical for early detection and treatment. Recent research in this field has leveraged machine learning and artificial intelligence to enhance skin cancer detection. This literature review surveys key papers from reputed journals, highlighting the proposed methods, technology, and their respective advantages and disadvantages.

Zhang and colleagues have published research on an innovative deep-learning framework for detecting skin cancer utilizing convolutional neural networks (CNNs). The team employed strategies such as transfer learning and data augmentation to enhance the model's efficacy. Their methodology has shown considerable success in accurately identifying skin lesions, indicating its applicability in medical settings. The research focuses on skin cancer detection through deep learning, specifically employing CNNs. These networks were trained using a substantial collection of dermoscopic images. A notable benefit of this approach is its achievement of accuracy comparable to that of dermatologists, which is significant for the development of automated diagnostic tools. The effectiveness of the model largely relies on the availability of a vast amount of labelled data and substantial computational power [15].

Ahmed et al. In their research work, the authors propose a multi-modal approach for skin cancer detection that combines dermoscopic images with clinical text descriptions. They employ recurrent neural networks (RNNs) for text analysis and CNNs for image classification, achieving improved accuracy by considering both modalities. The proposed method given an improved accuracy by leveraging complementary information and it requires access to clinical narratives, which may not always be available. This is the main drawback of the present study [16]. Li et al., in their research work, mainly focused on interpretability in skin cancer diagnosis [17]. The authors introduce attention mechanisms in their deep-learning model to highlight regions of interest in skin lesion images. Their approach not only predicts skin cancer but also provides visual explanations for the predictions, aiding dermatologists in their decision-making.

Dey et al. have proposed a work on Skin Lesion Classification Using an Ensemble of Fine-Tuned Deep CNN. Federated learning is explored in this paper as a privacy-preserving approach for skin cancer detection. The authors demonstrate how models can be trained across

multiple healthcare institutions without sharing sensitive patient data. Their approach addresses data privacy concerns while maintaining model accuracy [18]. J. Avanija et al. have proposed a work on Ensemble Learning for Skin Cancer detection using ensemble learning. This research investigates the benefits of ensemble learning in skin cancer classification. The authors combine multiple machine learning models to improve the robustness and accuracy of skin cancer prediction, highlighting the potential of ensemble methods in clinical applications. Using the ensemble approach, the author has Enhanced predictive performance and model robustness. Since multiple models are being used, there was some complexity in model selection and maintenance [19].

In this research paper, the author has demonstrated a paper on Skin Cancer Detection on Low-Resource Hardware Using Model Compression. This mainly focused on addressing the challenge of deploying skin cancer detection models on low-resource hardware, such as mobile devices or edge devices, where computational resources are limited [20], [21]. This implies that skin cancer detection can be performed efficiently on devices with limited computational power. Depending on the compression technique used, there may be a trade-off between model size and accuracy. Additionally, compression methods may introduce additional complexity during the compression process [22], [23].

The dermatoscopic patterns of AK, BD, and SCC were first delineated by the researcher in [24], where a comparative analysis of these patterns was conducted. This research proposed a model illustrating the progression from AK to BD and then to SCC, highlighting specific dermatoscopic observations at each stage, building upon prior studies. In our research, we delved into the dermoscopic characteristics of keratinocyte neoplasms and their dermatopathological associations. Additionally, he has suggested that these dermatoscopic features may be an indication of the vertical development phase as well as dermal invasion. When these symptoms are seen on dermatoscopy, a biopsy needs to be done to rule out the possibility of an invasive tumour. This is true regardless of whether the lesion is clinically flat or raised [24]-[26].

There is a correlation between "field cancerization," often known as areas of subclinical UV damage near AK lesions that have the same genetic abnormalities as AK, and multiple AK. [11]. In the case of keratinizing tumours, the ability to distinguish AK from the other keratinizing tumours is critical for deciding between ablative and other treatment modalities [27], [28]. In order to view four-dot clods, polarised dermatoscopy is necessary. The theory suggests that the interaction of polarized light with constricted or keratin-filled adnexal openings, along with the variation of localized hyperkeratosis and the normal corneal layer, plays a key role in dermatopathologic correlates [29]-[31]. Studies have posited that smaller four-dot clods result from concentric horns in the follicle at the infundibular level, whereas larger clods are attributed to concentric fibrosis surrounding the follicle [32]. This body of research highlights the variety of methods and technologies employed in skin cancer detection using machine learning and AI [33], [34]. Each technique presents unique strengths and weaknesses, and their appropriateness is contingent on the particular clinical and practical scenarios. These studies offer valuable insights for researchers and practitioners in refining their methods for diagnosing skin cancer.

3. Methodology

Skin cancer is among the deadliest. Deoxyribo Nucleic acid (DNA) in skin cells that has not been repaired can lead to the development of skin cancer. This situation could lead to genetic alterations or mutations in the skin. Given that the skin is the largest organ in the human body, it naturally follows that skin cancer is the most prevalent cancer among humans [2]. Skin cancer primarily manifests in two forms: melanoma and non-melanoma. Melanoma, identified as the gravest form of skin cancer, represents a substantial health hazard. Although less common, it is frequently associated with fatal outcomes for those affected. According to the American Cancer Society, the mortality rate associated with skin cancer overall is only one per cent, but the mortality rate associated with melanoma skin cancer is significantly higher. Melanoma begins in cells called melanocytes and spreads throughout the body. Everything starts off on the right foot when you're well. When melanocytes proliferate unchecked, the result is the formation of a cancerous tumour. It is possible for it to have an effect on every part of the human body. Hands, face, neck, lips, and other parts that are frequently exposed to the sun are common places where it might appear [11].

Since skin cancer has a tendency to progressively spread to other parts of the body, it is most curable when it is caught in its earlier stages. The middle and higher layers of the epidermis are where these three different forms of cancer are discovered. The likelihood of this particular form of cancer spreading to other parts of the body is relatively low. Melanoma malignancies, on the other hand, are more challenging to treat than non-melanoma tumours, which may be treated with more ease [28].

When it comes to the diagnosis of skin malignancies, deep neural networks are an extremely useful tool. A network links each individual node to the other nodes in the system. Their structure is comparable to that of the human brain in terms of the neuronal connections that are present.



Figure 1. Skin Disease Dataset from International Skin Imaging Collaboration

Their nodes work together to find solutions to various problems. In the end, neural networks achieve a level of expertise in the fields to which they were exposed during their training. During the course of our study, neural networks were educated to be able to categorize photos and distinguish between the many forms of skin cancer. The collection that was created by the International Skin Imaging Collaboration (ISIC) includes a wide variety of skin lesions, some of which are depicted in Figure 2. Non-melanoma cancers such as basal cell, squamous cell, and sebaceous gland carcinoma make up most cancer cases. Three epidermal cancers occur in the middle and higher layers. This cancer rarely spreads. Nonmelanoma tumours are easier to treat than melanoma tumours [29]. Due to these challenges, researchers have developed many skin cancer early detection approaches. Lesion criteria, including symmetry, colour, size, shape, etc., are used to diagnose and distinguish benign from melanoma skin cancer. The various processes involved in skin cancer detection are extensively studied in this research. The complete technique is presented in Figure 3.

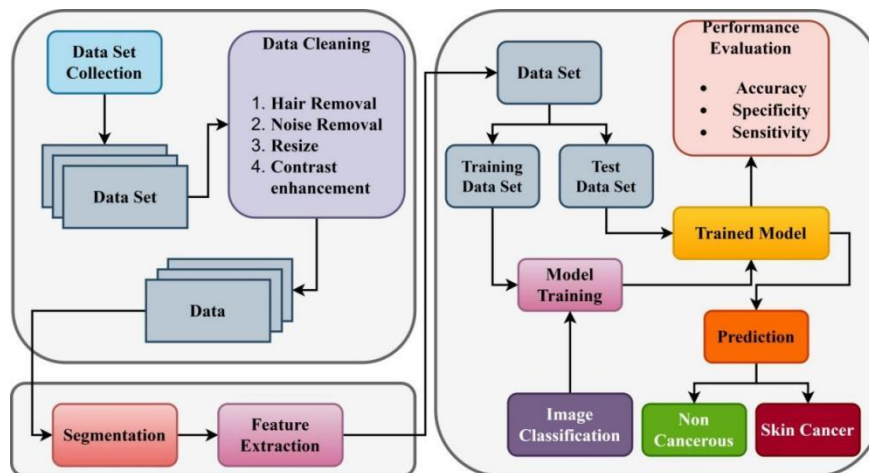


Figure 2. The Various Process Involved in the Detection of Skin Cancer

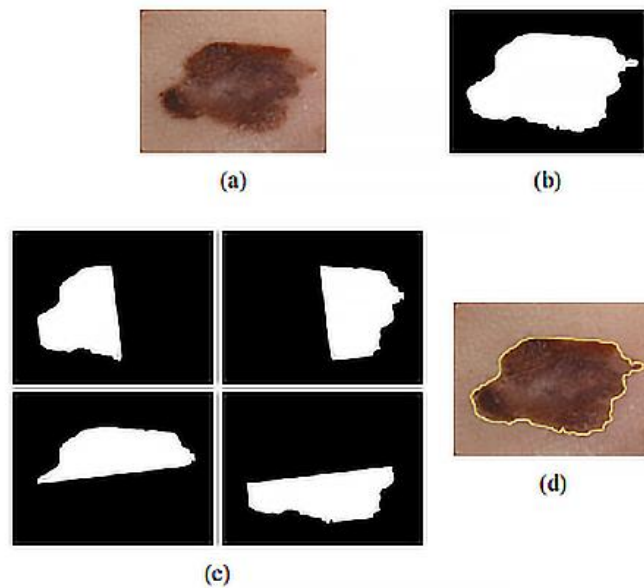


Figure 3. Melanoma Detection and Classification Based on the Proposed Method. Fig a) depicts The input image, fig b) corresponds to the identification of melanoma after removing skin and noise, fig c) represents semi planes formed to obtain symmetry, fig d) represents the edge detection.

The proposed method is depicted as pseudocode for skin colour identification (which is pre-processing). Feature extraction and classification are all part of the proposed method. Below, Algorithm 1 depicts the proposed method in pseudocode form. Figure 4 shows how the detection and classification of melanoma are done based on the proposed Algorithm 1 methodology.

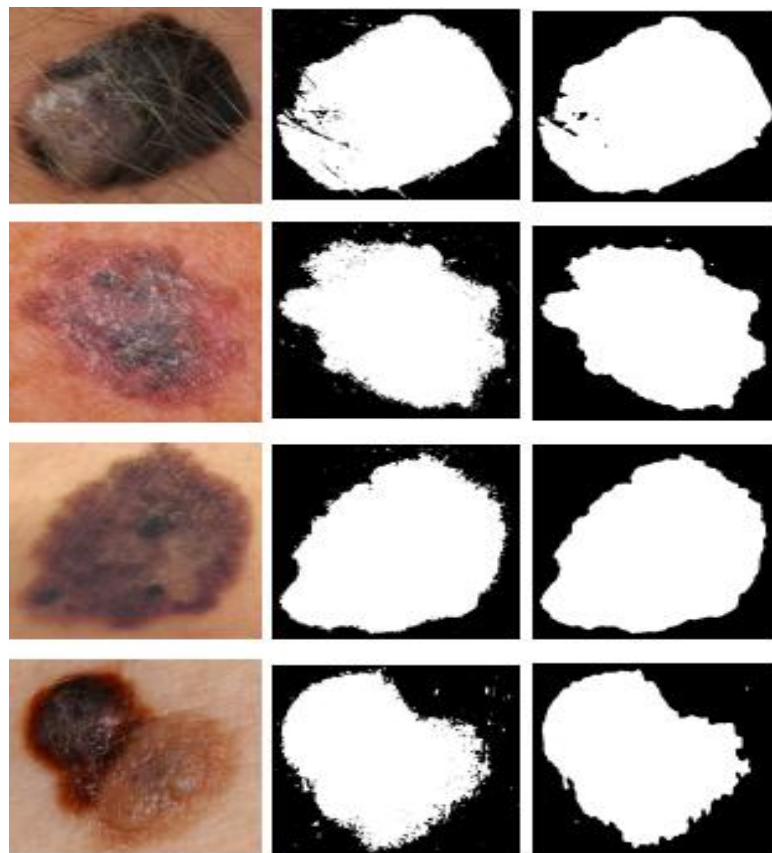


Figure 4. Removal of Skin and Noise from the Original Image. (a) Original Image, (B) Results Obtained after Applying the Gaussian Filter, and (c) Final Results obtained after applying Mathematical Morphology.

Algorithm 1. The proposed method shows the various stages, as shown in Figure 4

	Input: Input as an Image I _i
	Output: classifier output, o
1:	The proposed method (I _i)
2:	I _{b,n} = Preprocessing (I _i)
3:	For all n do
4:	a= get the symmetry(I _b)
5:	b= get the edge(I _b)
6:	c= get the color(I _b)
7:	a= get the size(I _b)
8:	o = $\begin{cases} \text{skin,} & \text{if MLP(a, b, c, d) = - 1} \\ \text{Benign,} & \text{if MLP(a, b, c, d) = 0} \\ \text{malignant,} & \text{Otherwise.} \end{cases}$
9:	I _e = Erosion (I _o , K1)
10:	I _d = Dilation (I _o , K2)
11:	Return I _d

3.1 Pre-processing Stage

In most computer vision algorithms, the main task is to remove the noise from the images. For that, the most common filter which is often used is the Gaussian filter. Gaussian smoothing filter is used to eliminate the noise and provides a uniform smoothing. The Gaussian function is described in Equation 1:

$$G_o(x,y) = Ae^{\frac{(x-\mu_x)^2}{2\sigma_x^2} - \frac{(y-\mu_y)^2}{2\sigma_y^2}} \tag{1}$$

In this context, μ represents the mean value (or the peak), A is a constant and refers to the standard deviation for the variables x and y , with (x,y) indicating the pixel coordinates. The process involves identifying and subsequently eliminating the skin colour from the image. This is achieved by transforming the image into the HSV (Hue, Saturation, Value) colour space. Each channel within this colour space is defined by its hue, saturation, and brightness levels, derived through a nonlinear conversion of the RGB colour space into cylindrical coordinates. To determine the skin color, color samples are collected from the image's corners after its conversion into the HSV space. Once the ranges and threshold levels have been established, these values are compared. Each image is examined to determine the subject's skin tone. As a result, each one has a different threshold range. The method works for all skin tones because the skin colour is created automatically. As a result of determining the colour ranges and thresholding, the skin appears black, but any suspected occurrences of melanoma are shown in white. The image noise is then reduced using a combination of Gaussian, morphological erosion, and dilation filters. Erosion occurs when a set of points (X) that represents a binary picture (X) is transferred into another set of points (x), with A (A') being the structuring element in both sets (X') (A'). This equation corresponds to dilatation in which A is the structuring element, X is the binary image, and P points at where A intersects X in relation to the reference point of the structuring element as in Equations 2 and 3 respectively:

$$\epsilon A(X) = \{x: Ax \subseteq X\} \tag{2}$$

$$\delta A(X) = \{p: Ap \cap X \neq \emptyset\} \tag{3}$$

Image conditioning, skin removal, and the identification of suspected melanoma instances are depicted in Algorithm 2's pseudo code. Figure 5 depicts four examples of melanoma screening and diagnosis.

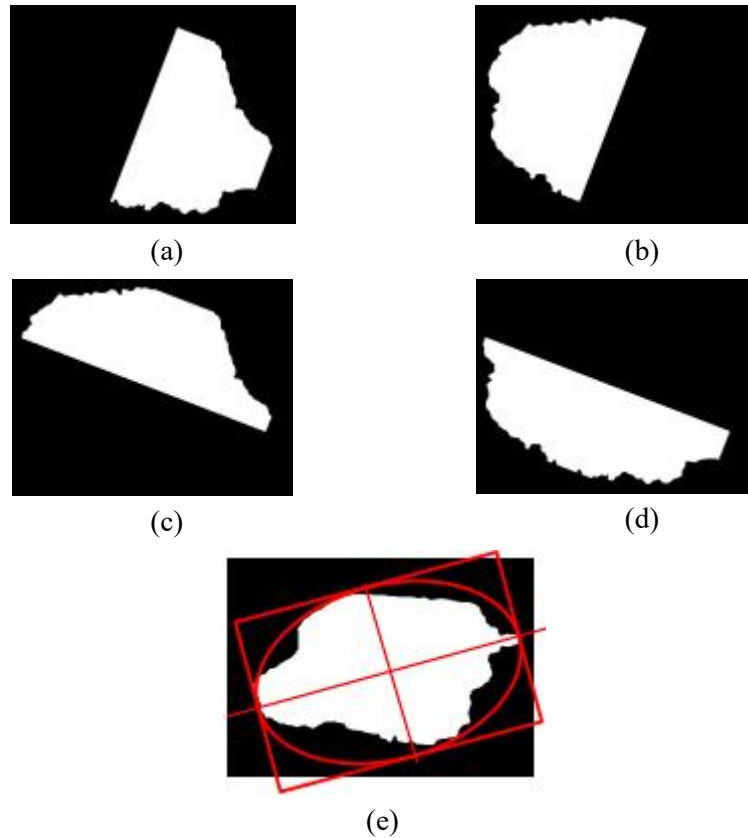


Figure 5. Symmetry and Shape Identification Test. (a,b) Comparison using the Smallest Axis. (c,d) Comparison using the Largest Axis. (e) The Contour of a Probable Melanoma Instance is outlined by an Ellipse and Rectangle, with Midpoints and Semiplanes Identified.

Algorithm 2. A method proposed to remove the noise and skin for the given image

Input: Input as an Image
Output: Skinless and Denoised image

```

1:      Preprocessing(Ii)
2:      Ig= GaussianBlur (Ii)
3:      Ic= conversion_RGB to HSV(Ig)
4:      H,s,v = Split Ic
5:      hmin,hmax = get_ranges corner(h)
6:      smin,smax = get_ranges corner(s)
7:      vmin,vmax = get_ranges corner(v)
8:      Io= zeros(size(h))
9:      For (x,y) ∈ h, do
10:     Io (x,y) = { 1,   hmin ≤ h(x,y) ≤ hmax
                  Smin ≤ S(x,y) ≤ Smax
                  Vmin ≤ V(x,y) ≤ Vmax
                  0,   Otherwise.
11:     Ie = Erosion (Io, K1)
12:     Id = Dilation (Io, K2)
13:     Return Id

```

3.2 Feature Extraction Stage

An algorithm based on the ABCD rule and Multilayer Perceptron Networks classifies images based on their descriptors. The ABCD rule is applied to the photographs taken with the phone's

camera, which uses only light that can be seen with the naked eye. The dataset, which included a variety of skin tones, was analysed using a Gaussian model to get its descriptors.

3.3 Symmetry (a)

To determine the symmetry of a suspected instance of melanoma, the contour is first detected, an ellipse is put, and last, the ellipse is inscribed. The ellipse is inscribed in a rectangle that has been formed. As soon as the rectangle has been created, the midpoints of each side are found, and the axes are positioned at these positions. The axes' semi-planes are compared in order to provide a weighting to each one. To begin, the image is divided into two semi-planes using the longest axis. Afterwards, the other axis is employed to perform the identical task. It is decided which of the two scores is the highest by comparing them. A score might have a maximum of 1 or a minimum of 0. The final value is fed into the multilayer perceptron, together with the size, colour, and edge information already mentioned. Figure 6 demonstrates an example of symmetry verification. The pseudo-code for evaluating symmetry is shown in Algorithm 3.

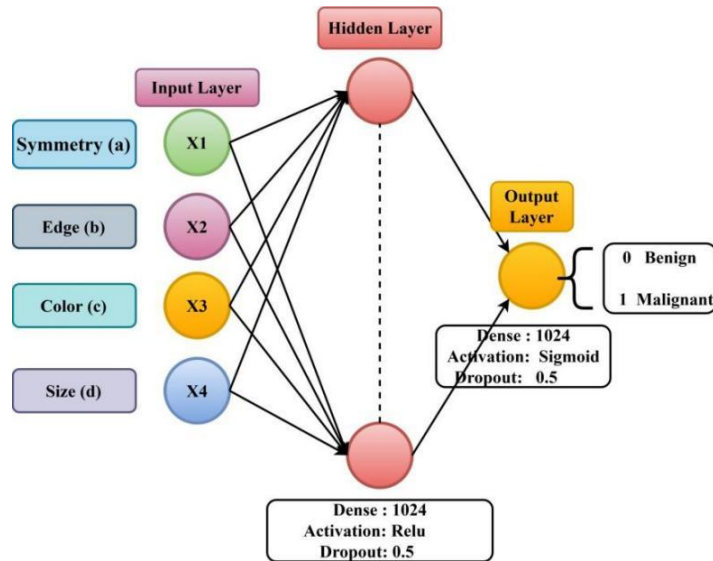


Figure 6. Proposed Multilayer Perceptron, four input data, and one output data.

Algorithm 3. To Evaluate the symmetry (a) from lines 1-14, as shown in Figure 6

Input: Input as an Image(Ii)
Output: a, Estimate value of symmetry

```

1: Procedure: Get the symmetry from the input Image(Ii)
2:   Ib= conversion_RGB to Gray (Ii)
3:   Ic= Get the contours(Ib)
4:   Id= circumscribed Ellipse(Ic)
5:   Ie= circumscribed Rectangle(Id)
6:   P= get the corners of Image(Ie)
7:   For all 4 semi plane(1,2,3,4) do
8:      $mp_{x0} = \frac{p[0,0]+p[1,0]}{2}$ 
9:      $mp_{y0} = \frac{p[0,1]+p[1,1]}{2}$ 
10:     $mp_{x2} = \frac{p[2,0]+p[3,0]}{2}$ 
11:     $mp_{y2} = \frac{p[2,1]+p[3,1]}{2}$ 
12:    Semi P1= semiplane (Ic, [p[0,0], p[0,1]], [mpx0, mpy0], [p[3,0], p[3,1]], [mpx2, mpy2])
    a1= similarity(SemiP1, SemiP2)
    a2= similarity(SemiP2, SemiP3)
    a= Highest of (a1, a2)
  return a

```

3.4 Edge (b)

Ultimately, the border's precision is meticulously verified, the contour is redefined, the area is computed, and the polygon that most accurately aligns with it is selected. This involves comparing the area of the polygon with that of the contour and then adjusting the quotient's result to align with the training data parameters. For detailed steps on contour estimation, the pseudocode is provided in Algorithm 6. The classifier uses the four descriptors as inputs once they have been estimated. Malignant melanoma, benign melanoma, and photographs of the skin are all outputs of this machine. The progression of malignant melanoma can be seen in the contour, which is shaded in accordance with the level of evolution. Malignancy. There are four severity levels, and the highest level corresponds to the descriptor with the biggest score.

3.5 Color(c)

Aspects of Design (c) You may get an idea of the colour dispersion (c) by looking at the h channel histogram. It is the combination of the colour space and channel that separates our description from those in the literature. The calculation of colour is shown in Algorithm 4, along with the pseudocode that goes with it.

Algorithm 4. To Evaluate the color dispersion(c) from line 1-9

Input: Input as an Image(Ii)
Output: d, Estimate value of color

```

1: Procedure: Get the color of the input Image(Ii)
2:   Ib= conversion_RGB to HSV (Ii)
3:   h,s,v = split the image into h,s,v (Ib)
4:   hist = get the histogram(h)
5:   c=0
6:   For each i=0 to 255, do
7:     If hist(i) ≠ 0 then
8:       C+= 1
9:   return c

```

3.6 Size (d)

A conditioned image contains all melanoma cases, which are quantified and the four ABCD rule descriptors are estimated for each conceivable melanoma case. Size is the first factor to be taken into account (d). In order to estimate the size, the contour is marked, the area is determined, and the quotient is computed. Melanoma is diagnosed by comparing the value acquired to the range established during training and, if necessary, evaluating the other descriptors. Otherwise, a new case of melanoma will not be discovered. In order to evaluate the size, we use Algorithm 5, which displays the corresponding pseudocode.

Algorithm 5. To Evaluate the size(d) from line 1-7.

Input: Input as an Image(Ii)
Output: d, Estimate value of edge

```

1: Procedure: Get the size of the input Image(Ii)
2:   Ib= conversion_RGB to Gray (Ii)
3:   Ic = Get the area of Contour (Ib)
4:   Id = Get the area (Ic)
5:   Ie = Get the area (Ii)
6:   d =  $\frac{Id}{Ie}$ 
7:   Return d

```

Design of a multilayered perceptron After the image has been conditionalised and the four descriptors have been approximated, the training and classification stage continues to be carried out. A multilayer perceptron is employed in this stage. One of the most common uses for this type of

neural network is for picture segmentation and pattern recognition. Layers 1 through n of the multilayer perceptron are all visible. A multilayer perceptron has a variety of inputs that are linked together.

Table 1 shows the many multilayer perceptron model configurations that were tried in order to find the optimal one. Numbers 1 through 3 represent input and output, respectively, while numbers 4 through 8 represent hidden layers. Design 4-1024-1 generally yields the best results. Figure 7 illustrates the designed architecture, consisting of three distinct layers: the input layer, equipped with four neurons corresponding to each descriptor of the ABCD rule; a middle layer featuring 1024 neurons; and a concluding layer containing a single neuron.

Table 1. Accuracy obtained from different MLP Architectures

MLP Architectures	Simple Images	Dermatological Images	Average
4-8-1	97.07	97.93	97.5
4-16-1	97.18	97.40	97.29
4-32-1	97.86	97.57	97.715
4-64-1	97.75	97.77	97.76
4-128-1	97.89	97.99	97.94
4-256-1	98.08	98.09	98.085
4-1024-1	98.57	98.65	98.61
4-16-16-1	98.26	98.77	98.515
4-32-32-1	98.18	97.88	98.03
4-64-64-1	98.07	98.17	98.12
4-128-128-1	98.18	97.40	97.79
4-256-256-1	97.99	98.16	98.075
4-1024-1024-1	98.33	98.19	98.26
4-16-16-16-1	98.10	97.40	97.75
4-256-256-256-1	98.36	98.10	98.23

This paper aims to conduct an analysis of the significance of descriptors in the context of the subject matter under investigation. The ABCD rule, a frequently utilized classification system in the literature, employs symmetry (a), edge (b), colour (c), and dimension (d) as descriptors to differentiate between benign and malignant melanoma. This rule has gained significant recognition due to its remarkable efficacy in producing accurate results. However, it is interesting to explore the importance of each descriptor in the multilayer perceptron that we have constructed. When utilizing a single descriptor, the most significant one is colour, with symmetry being the subsequent crucial characteristic. This observation is evident in the comparison presented in Table 2, which demonstrates that different configurations of descriptors yield diverse outcomes. When employing two descriptors, the most advantageous combination is one that encompasses both symmetry and dimension. When faced with three descriptors to pick from, the optimal combinations to employ are the edge, colour, and size.

Table 2. Accuracy obtained with different Descriptors Setup

Descriptor			Accuracy		
Symmetry(a)	Edge(b)	Color(c)	Dimension(d)	Simple	Dermatological
X	X	X	X	98.57	98.65
X	X	X		94.06	90.38
	X	X	X	95.74	94.80
X		X	X	93.03	93.40
X	X		X	94.09	92.38
X	X			91.04	90.2
	X	X		90.54	87.2
		X	X	90.31	8.63

X			X	91.09	92.08
X		X		93.14	89.94
	X		X	84.96	91.34
X				76.03	86.38
	X			72.48	83.67
		X		88.17	85.29
			X	70.85	84.74

3.7 Performance Evaluation

The performance evaluation of the algorithm will be based on two key metrics. The initial phase, termed cross-validation, is designed to refine the model's accuracy in distinguishing between malignant and benign melanoma cases. This involves employing the K-fold cross-validation technique, wherein the dataset is segmented into a training set and a validation set. Additionally, the training set is subdivided into ten distinct subsets. Throughout the training phase, each subset is used in rotation as a test set while the remaining data functions as the training set. The aforementioned procedure is repeated a total of ten times, with each iteration including the selection of a distinct test set. The remaining data is then employed as a training set for the respective iteration. The training dataset is utilized to enhance the precision of the model. During each cycle of the process, an assessment is made of the count of true negatives (TN), false negatives (FN), true positives (TP), and false positives (FP). These figures are then utilized to calculate key metrics: precision (formula 4), specificity (formula 5), sensitivity (formula 6), and efficiency (formula 7). Here, TN is indicative of true-negative cases, FN stands for false-negative instances, TP refers to true-positive scenarios, and FP represents false-positive occurrences.

Accuracy: Accuracy is defined as the combination of sensitivity and specificity of the model. Accuracy is defined as follows, as shown in the equation:

$$\text{Accuracy} = \frac{\text{TP} + \text{TN}}{\text{TP} + \text{TN} + \text{FP} + \text{FN}} \quad (4)$$

Specificity: Specificity is defined as the ability to correctly identify healthy people who do not have the condition. It is defined as in the equation:

$$\text{Specificity} = \frac{\text{TN}}{\text{TN} + \text{FP}} \quad (5)$$

Sensitivity: Sensitivity is defined as the ability to measure cases with their condition.

$$\text{Sensitivity} = \frac{\text{TP}}{\text{TP} + \text{FN}} \quad (6)$$

Efficiency is defined as the average of the above three and is as shown in the equation:

$$\text{Efficiency} = \frac{\text{Sensitivity} + \text{Specificity} + \text{Accuracy}}{3} \quad (7)$$

After further testing and assessing the quality of the photos for both groups, the textural properties of the images are extracted and categorised utilising many different sets of classifiers, including logistic regression and support vector machine. Moreover, the efficacy of these classifiers is corroborated through a technique named 10-fold cross-validation. During this process, various metrics, including accuracy, sensitivity, specificity, True Positive Rate, False Positive Rate, and the Receiver Operating Characteristics (ROC) with the Area Under the Curve (AUC), are computed. Table 3 presents an analysis of the confusion matrix, which encompasses True Positives, False Negatives, False Positives, and True Negatives, as depicted in Figure 8.

Table 3. Confusion Matrix for all Classifiers

Classifier	TP	FN	FP	TN
MLP	33	16	14	48
Quadratic SVM	31	18	16	46
Fine Gaussian SVM	28	21	10	52
Medium Gaussian SVM	25	24	13	49

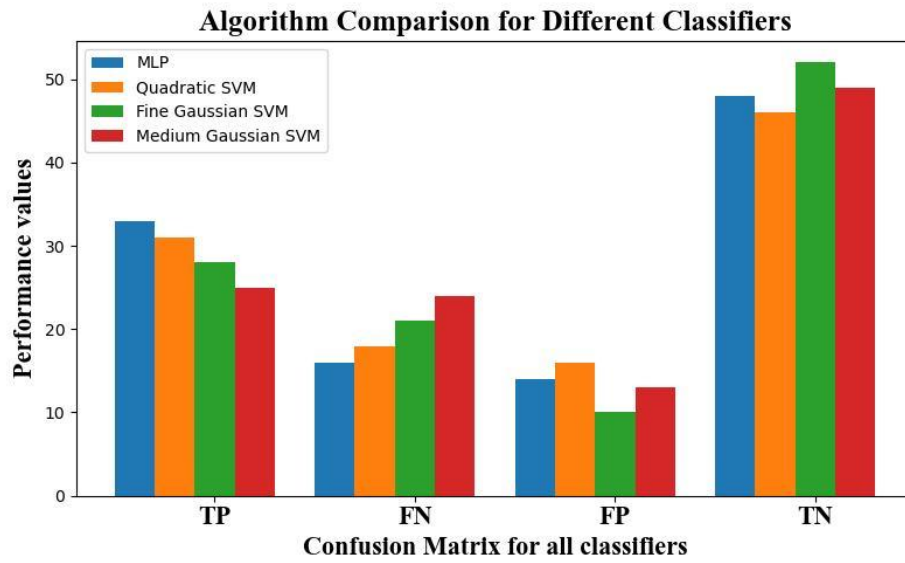


Figure 7. Classified Samples

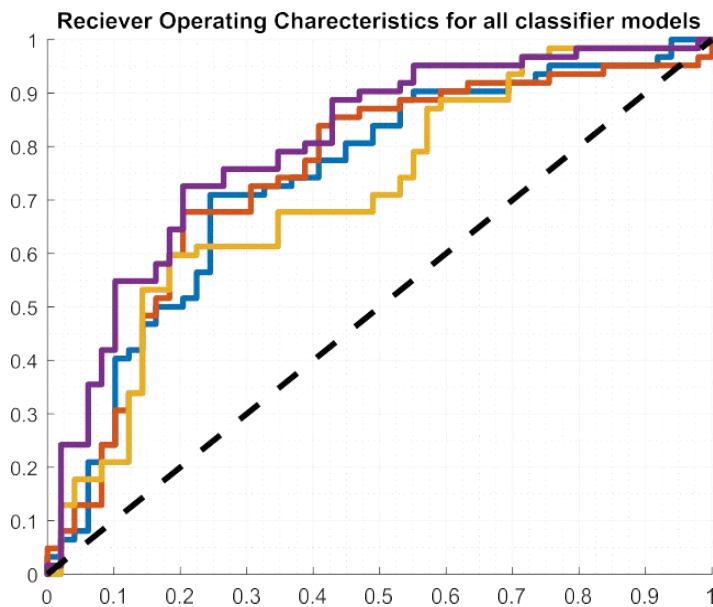


Figure 8. Receiving Operating Characteristics for all Classifier Models; Blue Line – Quadratic SVM; Red – Fine Gaussian SVM; Purple Line – Multi-Layer Perceptron; Yellow – Medium Gaussian SVM

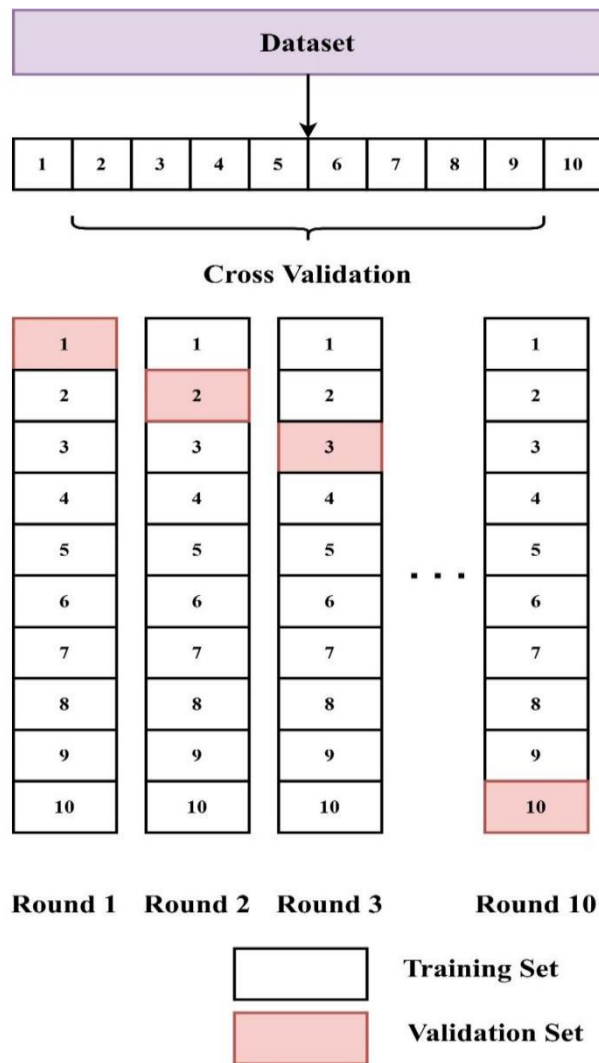


Figure 9. Cross-Validation, 10 Subsets are Randomly Selected

Additional classifier metrics are computed, including Accuracy, Sensitivity, Specificity, Positive Predicted Value, and Receiving Operating Characteristics, as shown in Table 3 and Figure 9. These metrics are described further below. After all of the iterations have been finished, the levels of efficiency and inaccuracy for each of the models that have been developed are figured out. In order to determine the efficiency as well as the overall inaccuracy, the average of the 10 different trained models is computed. The Cross-Validation procedure is depicted in Figure 9, which may be found here.

4. Results and Discussion

Image processing and a multilayer perceptron were used in this study to build an effective and robust technique for detecting melanomas in simple dermatological images. The ABCD rule's descriptors are estimated by the algorithm and fed into the multilayer perceptron as input. Malignant and benign melanoma are taught and classified under its auspices. It is responsible. Figure 10 and 11 show how the findings of the research help identify the shape and kind of melanoma (contour colour indicates severity). Malignant melanoma cases can also be classified according to their severity.

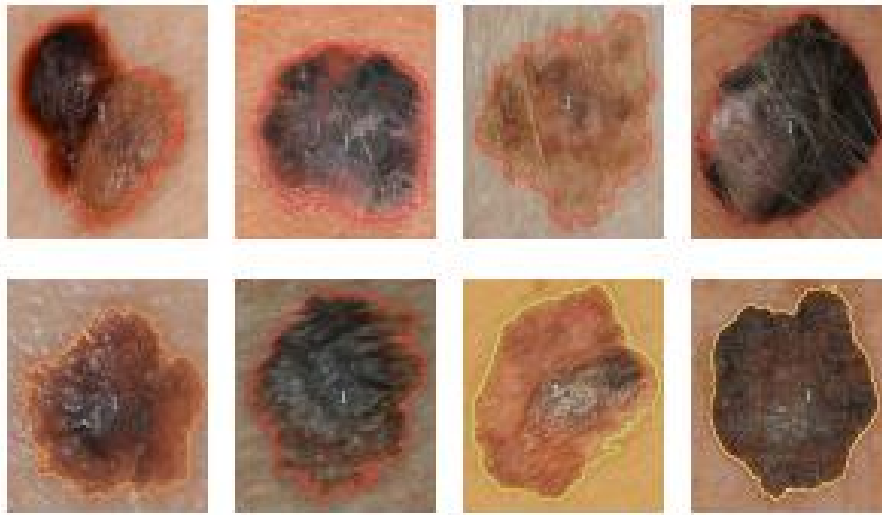


Figure 10. Examples of Identification and Classification of Malignant Melanoma Cases in Simple Images

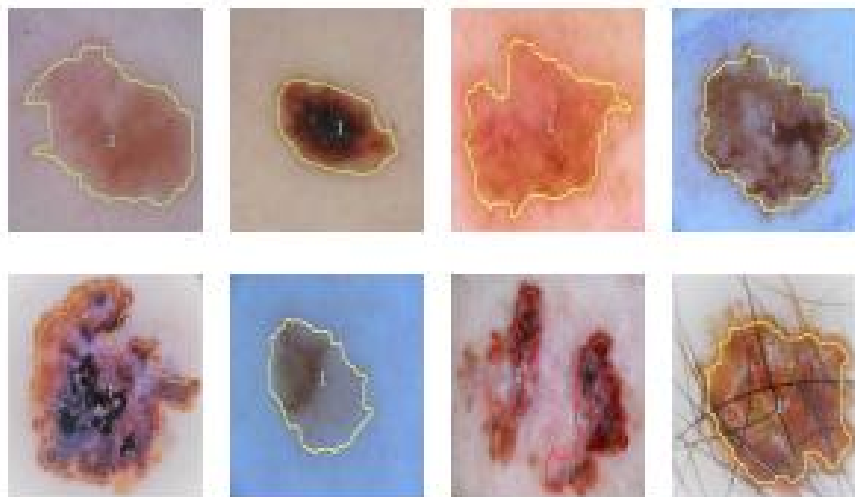


Figure 11. Examples of Identification and Classification of Malignant Melanoma Cases in Dermatological Images

The validation procedure was divided into two phases. The initial phase involved cross-validation using Equations (4)-(7), while the second phase focused on statistical data analysis. Post-application of these equations, the method achieved an efficiency rate of 97.78 per cent for basic images and 98.22 per cent for dermatological images. The results indicate that this method surpasses traditional approaches in terms of efficiency. The precision metrics obtained during the iterations for both basic and dermatological images are detailed in Table 4. Furthermore, Figure 12 illustrates a comparative analysis of the efficiency levels achieved by this method against other studies that utilized similar types of images and datasets, serving as a benchmark for evaluating the effectiveness of this approach.

Table 4. 10-Fold Cross Validation Accuracy

Type of Image	K=1	K=2	K=3	K=4	K=5	K=6	K=7	K=8	K=9	K=10	Average
Dermatological	97.89	98.15	100	97.23	100	97.9	100	98.41	97.86	99.11	98.65
Simple	98.27	99.01	96.89	99.30	100	97.98	98.77	99.34	98.16	98.02	98.57

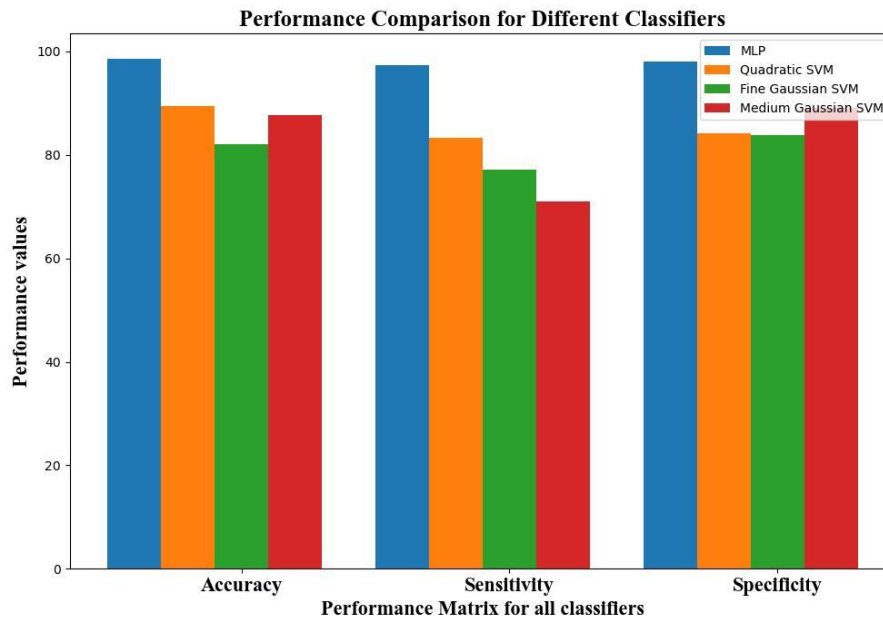


Figure 12. Comparison of Efficiency between Reported Literature and Proposed Approach

Once a malignant melanoma has been discovered, the next step in the classification process involves determining the level of severity associated with the disease. The classification is ascertained by considering both the highest and lowest values derived from each descriptor's estimation. For the second metric, the categorization for malignant melanoma cases is defined as level one for values under 0.35, indicated by a green colour; level two for values under 0.65, marked by yellow; level three for values under 0.85, represented by orange; and level four for values exceeding 0.85, depicted in red colour. Figure 10 and 11 provide examples of malignant melanomas at varying severity levels. Subsequently, the confidence levels of the mean were computed. The analysis concluded that, on average, the cases would fall within the 97 per cent confidence interval.

5. Conclusion

This study aimed to present a technique for identifying and classifying melanomas in both basic and dermatological images. The approach incorporates mathematical morphology, Gaussian filters, the HSV colour model, and a multilayer perceptron in its evaluation process. Assessments were conducted focusing on key attributes such as symmetry, dimensions, color, and boundary characteristics of the subject. The classification task within this framework is primarily handled by the multilayer perceptron. A number of experiments using the classifier with a variety of parameters were carried out. A sigmoidal activation function was used in conjunction with 1024 neurons in the hidden layer to produce the greatest results. The outcomes of the experiment obtained a performance that was more effective than the three contemporary methods.

References

- [1] H. Younis, M. H. Bhatti and M. Azeem, "Classification of Skin Cancer Dermoscopy Images using Transfer Learning," in *2019 15th International Conference on Emerging Technologies*, Peshawar, Pakistan, pp. 1-4, 2019.
- [2] A. Namozov and Y. I. Cho, "Convolutional Neural Network Algorithm with Parameterized Activation Function for Melanoma Classification," in *2018 International Conference on Information and Communication Technology Convergence*, pp. 417-419. 2018.
- [3] P. Dubal, S. Bhatt, C. Joglekar and S. Patil, "Skin cancer detection and classification," in *2017 6th International Conference on Electrical Engineering and Informatics (ICEEI)*, pp. 1-6, 2017
- [4] O. Ronneberger, P. Fischer, and T. Brox, "U-net: Convolutional networks for biomedical image segmentation," in *Medical Image Computing and Computer-Assisted Intervention—MICCAI 2015: 18th International Conference, Munich, Germany, October 5-9, 2015, Proceedings, Part III 18*. Springer International Publishing, 2015, pp. 234-241.

- [5] T. U. Ahmed, S. Hossain, M. S. Hossain, R. Ul Islam, and K. Andersson, "Facial expression recognition using convolutional neural network with data augmentation," in *2019 Joint 8th International Conference on Informatics, Electronics & Vision (ICIEV) and 2019 3rd International Conference on Imaging, Vision & Pattern Recognition (icIVPR)*, 2019, pp. 336-341.
- [6] K. N. Sunilkumar, G.A. Kumar, R. Gatti, S.S. Kumar, D.A. Bhyratae, and P. Satyasrikanth, "Design And Implementation Of Auto Encoder Based Bio Medical Signal Transmission To Optimize Power Using Convolution Neural Network," *Neuroscience Informatics*, p. 100121, 2023.
- [7] R. B. Oliveira, J. P. Papa, A. S. Pereira, and J. M. R. S. Tavares, "Computational methods for pigmented skin lesion classification in images: review and future trends," *Neural Computing and Applications*, vol. 29, no. 3, pp. 613-636, 2018.
- [8] K. Peris, M.C. Fargnoli, C. Garbe, R. Kaufmann, L. Bastholt, N.B. Seguin, V. Bataille, V. Del Marmol, R. Dummer, C.A. Harwood, and A. Hauschild, "Diagnosis and treatment of basal cell carcinoma: European consensus-based interdisciplinary guidelines," *European Journal of cancer*, vol. 118, pp. 10-34, 2019.
- [9] M. A. Wahba, A.S. Ashour, Y. Guo, S.A. Napoleon, and M.M. Abd Elnaby, "A novel cumulative level difference mean based GLDM and modified ABCD features ranked using eigenvector centrality approach for four skin lesion types classification," *Computer methods and programs in biomedicine*, vol. 165, pp. 163-174, 2018.
- [10] P. Carcagni, M. Leo, A. Cuna, P. Mazzeo, P. Spagnolo, G. Celeste, C. Distante, "Classification of Skin Lesions by Combining Multilevel Learnings in a DenseNet Architecture." in *Image Analysis and Processing-ICIAP 2019: 20th International Conference, Trento, Italy, September 9-13, 2019, Proceedings, Part I 20*, Springer International Publishing. 2019, pp. 335-344.
- [11] S. C. Hames, S. Sinnya, J.M. Tan, C. Morze, A. Sahebian, H.P. Soyer, and T.W. Prow, "Automated detection of actinic keratoses in clinical photographs," *PLoS One*, vol. 10, no. 1, p. e0112447, 2015.
- [12] L. Ballerini, R.B. Fisher, B. Aldridge, J. Rees, "A color and texture based hierarchical K-NN approach to the classification of non-melanoma skin lesions," *Color Medical Image Analysis*, pp. 63-86. 2013.
- [13] N. Georgopoulos, D. Stavrakoudis and I. Z. Gitas, "Object-Based Burned Area Mapping Using Sentinel-2 Imagery and Supervised Learning Guided by Empirical Rules," in *IGARSS 2019-2019 IEEE International Geoscience and Remote Sensing Symposium*, IEEE, Jul.2019, pp. 9980-9983.
- [14] J. F. Alcón, C. Ciuhu, W. Ten Kate, A. Heinrich, N. Uzunbajakava, G. Krekels, D. Siem, and G. de Haan, "Automatic imaging system with decision support for inspection of pigmented skin lesions and melanoma diagnosis," *IEEE journal of selected topics in signal processing*, vol. 3, no. 1, pp. 14-25, 2009.
- [15] L. Zhang, H.J. Gao, J. Zhang, and B. Badami, "Optimization of the convolutional neural networks for automatic detection of skin cancer," *Open Medicine*, vol. 15, no. 1, pp. 27-37, 2020.
- [16] I.A. Ahmed, E.M. Senan, H.S.A. Shatnawi, Z.M. Alkhraisha, M.M.A. Al-Azzam, "Multi-Models of Analyzing Dermoscopy Images for Early Detection of Multi-Class Skin Lesions Based on Fused Features," *Processes*, vol. 11, no. 3, p. 910, 2023.
- [17] W. Li, W. Mo, X. Zhang, Y. Lu, J.J. Squiers, E.W. Sellke, W. Fan, J.M. DiMaio, and J.E. Thatcher, "Burn injury diagnostic imaging device's accuracy improved by outlier detection and removal," in *Algorithms and technologies for multispectral, hyperspectral, and ultraspectral imagery XXI*, vol. 9472, SPIE, May. 2015, pp. 58-68.
- [18] Dey., "Skin Lesion Classification Using Ensemble of Fine-Tuned Deep Convolutional Neural Networks," in *Proceedings of the IEEE International Conference on Computer Vision*, vol. 86, 2018, pp.25-32.
- [19] J. Avanija, C. C. M. Reddy, C.S.C. Reddy, D.H. Reddy, T. Narasimhulu and N.V. Hardhik, "Skin Cancer Detection using Ensemble Learning," in *2023 International Conference on Sustainable Computing and Smart Systems (ICSCSS)*, 2023, pp. 184-189.

- [20] S.K. KN and S. Shivashankar, "Compression of PPG Signal through Joint Technique of Auto-encoder and Feature Selection," *International Journal of Health Care Information Systems and Informatics-ESCI Indexed ACM-Digital Library*, vol. 16, no. 4, pp. 1-15, 2021.
- [21] S. K. Shivashankar, "Bio-signals Compression Using Auto Encoder," *Journal of Electrical and Computer Engineering (Q2 Indexed)*, Institute of Advanced Engineering and Science publishers, vol.11, no.1, pp. 424-433. 2021.
- [22] Sunil Kumar K N and Shivashankar, "Security Framework for Physiological Signals using Auto Encoder," *Journal of Advanced Research in Dynamical and Control Systems – (Q3 Indexed)*, vol. 12, no. 01, pp. 583-592, 2020.
- [23] S. K. KN, R. Sathish, S. Vinayak and T. P. Pandit, "Braille Assistance System for Visually Impaired, Blind & Deaf-Mute people in Indoor & Outdoor Application," in *2019 4th International Conference on Recent Trends on Electronics, Information, Communication & Technology (RTEICT)*, 2019, pp. 1505-1509.
- [24] R. Gatti, N. Nataraja, T. Sarala, S. S. Kumar, R. P. Prasad and S. K. N. Kumar, "Development of Automated System for Detection of Diabetic Retinopathy," in *2021 International Conference on Recent Trends on Electronics, Information, Communication & Technology (RTEICT)*, 2021, pp. 943-946.
- [25] H. A. Haenssle, C. Fink, R. Schneiderbauer, F. Toberer, T. Buhl, A. Blum, A. Kalloo, A.B. Hassen, L. Thomas, A. Enk, and L. Uhlmann. "Man against machine: diagnostic performance of a deep learning convolutional neural network for dermoscopic melanoma recognition in comparison to 58 dermatologists," *Annals of oncology*, vol. 29, no. 8, pp. 1836-42, 2018.
- [26] N. N. Sultana, and N.B. Puhan, "Recent deep learning methods for melanoma detection: a review," in *Mathematics and Computing: 4th International Conference, ICMC 2018, Varanasi, India, January 9-11, 2018, Revised Selected Papers 4*. Springer Singapore, 2018, pp. 118-132.
- [27] J. F. Alcón, C. Ciuhu, W. Ten Kate, A. Heinrich, N. Uzunbajakava, G. Krekels, D. Siem, G. de Haan, "Automatic imaging system with decision support for inspection of pigmented skin lesions and melanoma diagnosis," *IEEE journal of selected topics in signal processing*, vol. 3, no. 1, pp. 14-25, 2009.
- [28] A. Steiner, M. Binder, M. Schemper, K. Wolff, and H. Pehamberger, "Statistical evaluation of epiluminescence microscopy criteria for melanocytic pigmented skin lesions," *Journal of the American Academy of Dermatology*, vol. 29, no. 4, pp. 581-588, 1993.
- [29] A. Steiner, H. Pehamberger, and K. Wolff, "In vivo epiluminescence microscopy of pigmented skin lesions. II. Diagnosis of small pigmented skin lesions and early detection of malignant melanoma," *Journal of the American Academy of Dermatology*, vol. 17, no. 4, pp. 584-591, 1987.
- [30] M. Phillips, H. Marsden, W. Jaffe, R.N. Matin, G.N. Wali, J. Greenhalgh, E. McGrath, R. James, E. Ladoyanni, A. Bewley, and G. Argenziano, "Assessment of Accuracy of an Artificial Intelligence Algorithm to Detect Melanoma in Images of Skin Lesions," *JAMA Network Open*, vol. 2, no. 10, pp. e1913436-e1913436, Oct. 2019.
- [31] C. J. McCormack, J. W. Kelly, and A.P. Dorevitch, "Differences in age and body site distribution of the histological subtypes of basal cell carcinoma. A possible indicator of differing causes," *PubMed*, vol. 133, no. 5, pp. 593-6, 1997.
- [32] H. L. Haller, M. Giretzlehner, J. Dirnberger, and R. Owen, "Medical documentation of burn injuries," in *Handbook of Burns*, M. G. Jeschke, L. P. Kamolz, F. Sjöberg, and S. E. Wolf, Eds. Vienna, Austria: Springer, 2012.
- [33] M. S. Badea, C. Vertan, C. Florea, L. Florea, and S. Bădoiu, "Automatic burn area identification in color images," in *2016 international conference on communications (COMM)*, Jun. 2016, pp. 65-68.
- [34] A. D. Jaskille, J. W. Shupp, M. H. Jordan, and J. C. Jeng, "Critical review of burn depth assessment techniques: Part I. Historical review," *Journal of burn care & research*, vol. 30, no. 6, pp. 937-947, 2009.